Pakistan Veterinary Journal

ISSN: 0253-8318 (PRINT), 2074-7764 (ONLINE)
DOI: 10.29261/pakvetj/2025.305

RESEARCH ARTICLE

The Conserved Stem-Loop II Motif Is Not Essential but Influences Replication of Porcine Astrovirus

Yuhang Luo[123], Yijie Liao[123], Wenting Zhang[123], Yiyang Du[123], Shiqin Yi[123], Kang Ouyang[123], Ying Chen[123], Zuzhang Wei[123], Qingting Dong[4*], Yifeng Qin[4*] and Weijian Huang [4*]

[1]Laboratory of Animal Infectious Diseases and Molecular Immunology, College of Animal Science and Technology, Guangxi University, Nanning, China; [2]Guangxi Zhuang Autonomous Region Engineering Research Center of Veterinary Biologics, Nanning, China; [3]Guangxi Key Laboratory of Animal Reproduction, Breeding and Disease Control, Nanning, China; [4]Guangxi Vocational University of Agriculture, Nanning, China
*Corresponding author: 562422415@qq.com; qinyf@gxu.edu.cn; huangweijian-1@163.com

ARTICLE HISTORY (25-873)

Received: September 07, 2025
Revised: October 30, 2025
Accepted: November 03, 2025
Published online: December 02, 2025

Key words:
Porcine astrovirus
Reverse genetics system
RNA structure
Stem-Loop II Motif

ABSTRACT

Porcine astrovirus (PAstV) is widespread in swine, yet the role of its conserved Stem-Loop II motif (s2m) remains unclear. Using a PAstV-GX1 reverse-genetics system, we engineered s2m deletions and point mutants and assessed replication and innate sensing in PK 15 cells. All mutants were viable and genetically stable. Compared with wild type, s2m-edited viruses showed attenuated early replication and delayed ORF2 accumulation, with growth converging by ~24 h post-infection. Disruption of s2m also advanced innate responses, increasing IFN-β mRNA and promoter activity at 8 h. Preinfection with an s2m mutant transiently restricted heterologous virus replication. These findings indicate that s2m is non-essential but optimizes early kinetics and tempers interferon activation, supporting its consideration as a structurally constrained, potentially targetable RNA element.

To Cite This Article: Luo Y, Liao Y, Zhang W, Du Y, Yi S, Ouyang K, Chen Y, Wei Z, Dong Q, Qin Y and Huang W, 2025. The conserved stem-loop ii motif is not essential but influences replication of porcine astrovirus. Pak Vet J. http://dx.doi.org/10.29261/pakvetj/2025.305

INTRODUCTION

Porcine astrovirus (PAstV), a member of the Astroviridae family, is a positive-sense, single-stranded RNA virus that primarily infects pigs, causing significant health issues and economic losses (Cortez *et al*., 2019; Dong *et al*., 2023; Liu *et al*., 2023). PAstV is notorious for causing gastrointestinal disturbances such as diarrhea and vomiting, and in more severe cases, it can lead to neurological symptoms like encephalitis (De Benedictis *et al*., 2011; Mendenhall *et al*., 2015; Porto *et al*., 2023). The PAstV genome, ranging from approximately 6.8 to 7.3 kb in length, encodes essential non-structural and structural proteins across three major open reading frames (ORF1a, ORF1b, and ORF2)(Arias and Dubois, 2017; Cortez *et al*., 2019; Du *et al*., 2021). The capsid protein, encoded by ORF2, is crucial for viral assembly and is a primary target of the host immune response, which highlights its potential as a focus for vaccine development (Bonaldo *et al*., 2002; Qin *et al*., 2018). PAstV is highly prevalent in pig populations worldwide, particularly affecting young piglets and leading to high morbidity and mortality rates (Arruda *et al*., 2017; Ulloa and Gutierrez, 2010). The clinical symptoms associated with PAstV, including severe diarrhea and dehydration, result in substantial economic losses for the swine industry each year (Fang *et al*., 2019). The ability of PAstV to cause encephalitis indicates a broader tropism beyond the gastrointestinal tract, complicating control measures. Furthermore, the virus exhibits extensive genetic diversity, with multiple genotypes co-circulating within populations, which further complicates the development of effective vaccines and antiviral strategies (Blomstrom *et al*., 2010; Liu *et al*., 2020; Pfaff *et al*., 2017; Reuter *et al*., 2018; Rivera *et al*., 2010).

The Stem-Loop II Motif (s2m) is a conserved RNA secondary structure found in the 3' untranslated region (UTR) of a variety of RNA viruses, including astroviruses, coronaviruses, and picornaviruses (Goebel *et al*., 2004; Jiang *et al*., 2023; Keep *et al*., 2023; Kofstad and Jonassen, 2011). While its role is thought to contribute to RNA stability, translation efficiency, and immune evasion in some viruses, the functional importance of s2m is not universally conserved. In certain viral families, such as coronaviruses, s2m appears to play a more variable role. For instance, studies on SARS-CoV-2 have demonstrated that while s2m is present in the viral genome, its removal does not significantly impact viral replication, suggesting that in this case, the motif may be dispensable (Huston *et*

al., 2021; Keep *et al*., 2023; Robertson *et al*., 2005). This finding highlights the potential redundancy or context-dependent nature of s2m's function across different viruses. In contrast, in other viruses like astroviruses and picornaviruses, s2m is more integral to viral replication, enhancing RNA stability and facilitating interactions with host cellular factors to promote efficient replication and immune evasion (Cunningham *et al*., 2023a; Imperatore *et al*., 2022). While s2m is not strictly essential for replication in some viruses, its influence on viral fitness and immune modulation underscores its importance as a target for antiviral strategies, albeit with the recognition that its impact can vary greatly depending on the virus and host context (Gilbert and Tengs, 2021; Lulla *et al*., 2021). The precise mechanisms by which s2m functions, and the degree of its necessity, remain areas of active investigation (Tengs *et al*., 2013; Tengs and Jonassen, 2016).

In our study, we employed reverse genetics and site-directed mutagenesis to construct s2m mutants of PAstV to explore the motif's impact on the virus's biology. By analyzing these mutants, we assessed their effects on viral growth kinetics, protein expression, and host immune response. Our results revealed that while s2m is not strictly necessary for PAstV replication, alterations in the motif significantly impair replication efficiency, decrease viral protein production, and induce an earlier and more robust type I interferon response. These findings underline the crucial role of s2m in optimizing PAstV replication and immune evasion, suggesting its potential as a target for novel antiviral strategies aimed at enhancing host defenses. This study not only deepens our understanding of PAstV biology but also contributes broadly to the field of virology by illustrating the varied functions of s2m across different viral infections. By highlighting the role of s2m in viral pathogenesis and host interaction, we pave the way for future research focused on exploiting this conserved RNA structure to develop more effective antiviral therapies.

MATERIALS AND METHODS

Virus Strains and Cells: The PAstV-GX1 strain (GenBank KF787112), isolated in 2013 from a diarrheic pig in Nanning, Guangxi (Fang *et al*., 2019), was passaged and stabilized in PK 15 cells. PK 15 cells (porcine kidney epithelium) and IPEC-J2 cells (porcine jejunal/intestinal epithelium) were cultured in DMEM supplemented with 10% heat-inactivated FBS at 37°C with 5% CO_2; IPEC-J2 culture conditions were identical to those used for PK 15. Unless otherwise indicated, infections included 0.5 mg/mL TPCK-treated trypsin during inoculation to facilitate viral entry (Zhang *et al*., 2021). BHK cells (hamster kidney) were maintained under identical conditions. For transfection, BHK cells at 70–80% confluence in 6-well plates were transfected with plasmids using Lipofectamine 3000 per the manufacturer's instructions; medium was replaced 6 h post-transfection with fresh DMEM/10% FBS. The PAstV-GX1 stock titer was $1\times10^{7.3}$ $TCID_{50}$/mL, providing a robust inoculum for replication and host–virus interaction assays.

Prediction of the s2m Secondary Structure in the PAstV-GX1 Strain: The RNA secondary structure of the s2m motif within the PAstV-GX1 strain was accurately predicted using the RNAfold software, part of the ViennaRNA Package (version 2.4). RNAfold utilizes the Minimum Free Energy (MFE) principle to predict base pairings within the s2m sequence, effectively generating a detailed secondary structure diagram while also calculating the associated free energy values. To further ensure the precision and reliability of these predictions, we also employed mfold software for cross-validation.

RNA Extraction, cDNA Synthesis and Quantitative PCR (qPCR): Total RNA was extracted from infected cells using Trizol reagent (Takara, JPN). After reverse transcription of the RNA to synthesize complementary DNA (cDNA), quantitative PCR (qPCR) was conducted using SYBR Green-based assays. The qPCR included absolute quantification targeting the ORF2 gene to measure viral RNA levels and assess replication efficiency. Additionally, relative quantification of the IFN-β gene was performed to evaluate host immune response upon infection（Table 1）.

Table 1: Primer sequences for constructing the s2m deletion and mutant plasmids.

Primer name	Primer sequences (5′-3′)
s2m-25-43-F	ACGCCGAGTAGACTTCTTTTCTGTC
s2m-25-43-R	AGAAAAGAAGTCTACTCGGCGTGGC
s2m-25-33-F	CACGCCGAGTAGTACAGCTTTCAC
s2m-25-33-R	GAAAGCTGTACTACTCGGCGTGGC
s2m-C12G-F	GAAAGCCGAGGgCACGCCGAGTAG
s2m-C12G-R	CTACTCGGCGTGcCCTCGGCTTTC
s2m-C18G-F	AGGCCACGCgGAGTAGGATC
s2m-C18G-R	ATCCTACTCcGCGTGGCCTC
ORF2-Xho I-F	CCAGTGGGAAGACGGAGctcgagGC
ORF2-Sac II-R	TCCccgcggTTTTTTTTTTTTTT
ORF2-6127-F	TTCCACATAGTGATACCAACAAAG
ORF2-6669-R	GCTTCTAATTAAATCAATTCTAAT
po-IFN-β-F	AGTGCATCCTCCAAATCGCT
po-IFN-β-R	GCTCATGGAAAGAGCTGTGGT
po-β-actin-F	GTGATCTCCTTCTGCATCCTGTC
po-β-actin-R	GCAAGAACTCACAGGACAGGAA

PAstV reverse genetics system: In constructing a reverse-genetics system for PAstV-GX1 (Qin *et al*., 2018), we used mFold (http://www.mfold.org/) to identify the s2m motif and predict its RNA secondary structure under a minimum-free-energy model. To interrogate function, we generated infectious clones bearing deletions 25–43 nt downstream of the ORF2 stop codon and point substitutions at conserved stem residues (Table 1).

Clones were assembled by splice-overlap–extension (SOE) PCR. The engineered genome was split into two RT-PCR fragments carrying the desired s2m edits and complementary overlaps. Fragments were first fused in a primer-free SOE step to promote overlap annealing/extension, followed by amplification of the full-length product with external primers ORF2-XhoI-F and ORF2-SacII-R (Du *et al*., 2021a; Du *et al*., 2021b; Liu *et al*., 2023). Resulting plasmids were validated by restriction analysis and Sanger sequencing, confirming precise incorporation of the s2m edits and genome integrity (Du *et al*., 2021; Liu *et al*., 2023).

Viral Titer Determination and Growth Curve Analysis: Cells in 96-well plates were grown to 70–80% confluence, washed with PBS, and inoculated with 10-fold serial dilutions of virus (seven dilutions; 100 µL/well; six

wells/dilution); maintenance medium alone served as the negative control. After 48 h, CPE was scored and infectious titers expressed as $TCID_{50}$/mL using the Reed–Muench calculation (Stanic, 1963). For multi-step growth analysis, passage-6 (P6) s2m-deletion and point-mutant viruses were used to infect PK-15 or porcine intestinal epithelial IPEC-J2 cells in 12-well plates at an MOI of 0.01. Following 1 h adsorption at 37°C with gentle agitation every 15 min, inocula were removed, monolayers were washed, and 1mL maintenance medium was added. Supernatants were collected at 4, 8, 12, 24, 36, 48, and 60 h post-infection and quantified by endpoint titration ($TCID_{50}$) to generate growth curves comparing wild-type and mutant strains in both cell types.

Flow Cytometry analysis of PAstV ORF2: PK 15 cells were infected with WT or mutant PAstV-GX1 (MOI = 0.01). At indicated time points, cells were harvested, fixed with 4% PFA for 20 min, permeabilized with 0.1% Triton X-100 for 10 min, and blocked with 5% BSA for 30 min. Cells were incubated with anti-ORF2 mAb (1:200) for 1 h at 37°C, followed by Alexa Fluor 488-conjugated secondary Ab (1:500) for 30 min in the dark. Samples were analyzed on a BD FACSCanto II (BD Biosciences) and 10,000 events were acquired per sample. Data were processed with FlowJo (Tree Star), and the percentage of $ORF2^+$ cells together with mean fluorescence intensity (MFI) were quantified.

Immunofluorescence Assays (IFA): To evaluate viral protein localization and expression levels, PK 15 cells were infected with both wild-type and mutant PAstV strains at an MOI of 0.01. At 48 hours post-infection (hpi), the inoculum was removed, and the cell monolayer was washed three times with phosphate-buffered saline (PBS). Cells were then fixed with ice-cold methanol at −20°C for 30 minutes. After fixation, cells were washed five times with PBS and incubated with a primary antibody (anti-ORF2C pcAb) at a dilution of 1:200 at 37°C for 2 hours. Following incubation with the primary antibody, cells were washed five times with PBS and then incubated with a secondary antibody (goat anti-mouse IgG H&L Alexa Fluor 488; Proteintech Inc., CHN) at 37°C for 1 hour. Cells were again washed five times with PBS and stained with DAPI (Solarbio Inc., China) for 5 minutes to visualize the nuclei. Finally, the cells were observed under a fluorescence microscope.

Western blotting: Total protein was extracted from PK 15 cells infected with wild-type or s2m-C18G-8 PAstV at indicated time points using RIPA buffer supplemented with 1% PMSF (Servicebio, Wuhan, China). Lysates were clarified (12,000 ×g, 15 min), quantified by BCA assay (Beyotime, Shanghai, China), mixed with loading buffer, and denatured (98°C, 15 min). Equal protein (30 μg) was resolved by SDS–PAGE and transferred to PVDF (250 V, 30 min). Membranes were blocked with 5% BSA in PBST (25°C, 1 h), incubated overnight at 4°C with PAstV monoclonal and β-actin primary antibodies, washed three times with TBST, and probed with HRP-conjugated secondary antibodies (37°C, 1 h). Bands were visualized by chemiluminescence (Cowin Biotech, Jiangsu, China) and analyzed using Image Lab (Bio-Rad, USA).

Dual-Luciferase Reporter Assay: To assess the effect of s2m alterations on interferon-beta (IFN-β) promoter activity, PK 15 cells were seeded into 12-well plates at 70% confluence. Cells were transfected with 350 ng of the po-IFN-β-luc reporter plasmid and 50 ng of the pRL-TK plasmid per well. After 6 hours of transfection, the culture medium was replaced, and cells were washed three times with PBS. Cells were then infected with PAstV-GX1 and its mutant strains at an MOI of 0.01 for 1 hour. Following infection, cells were maintained in serum-free DMEM containing 0.5 μg/mL TPCK-treated trypsin. Cell lysates were collected at 4, 8, 12, and 24 hours post-infection (hpi), and luciferase activity was measured according to the manufacturer's instructions.

VSV-GFP interferon-bioactivity assay: PK 15 cells were seeded in 12-well plates and infected with PAstV-GX1 wild type or the indicated s2m mutants at an MOI of 0.01. After 1 h adsorption at 37 °C with gentle mixing every 15 min, inocula were removed and replaced with maintenance medium. Culture supernatants collected at 4, 8, 12, and 24 h post-infection were UV-inactivated to abrogate residual PAstV. In parallel, PK 15 cells in 24-well plates (~80% confluence) were overlaid with the inactivated supernatants for 24 h at 37°C, then challenged with VSV-GFP at the indicated MOI. Native GFP fluorescence was imaged 24 h post-challenge by epifluorescence microscopy under identical acquisition parameters (Ex 488 nm, Em 507 nm).

Statistical analysis: Data analysis was performed using Prism 9.3.1 (GraphPad). Data were plotted using this software, and both parametric and non-parametric comparisons were made where appropriate. Post-hoc analyses following Kruskal-Wallis tests were conducted using Dunn's multiple comparisons test to adjust for multiple comparisons. For the multi-step growth curves, the data were log-transformed and analyzed using two-way ANOVA in Prism, after excluding the 1-hour time point, to compare mutants with PAstV-GX1.

RESULTS

Structural Analysis and Mutagenesis of the s2m Motif in PAstV-GX1: A multiple sequence alignment of s2m from representative astroviruses showed marked conservation of the 3′-UTR-embedded module, with highest conservation across the core hairpin and flanking stems and limited divergence largely in loop or boundary regions (Fig. 1A). In PAstV-GX1, s2m maps to nt 6565–6607 at the ORF2–3′UTR junction and is predicted by Mfold to form a canonical stem–loop with two internal loops and three stem segments (Fig. 1B). Notably, the ORF2 stop codon is centrally embedded within the fold, suggesting a potential role in coupling translation termination with 3′-end RNA architecture.

To probe function, we engineered precise deletions (Δ25–43 and Δ25–33 relative to the ORF2 stop) and point substitutions at conserved stem positions (C12G, C18G) designed to perturb base-pairing. Refolding of mutant RNAs in Mfold indicated shifts in minimum free energy (MFE) and local topology relative to WT, including reorganization of internal loops and predicted weakening of stem stability (Fig. 1C). These in silico findings guided reverse-genetics construct selection (Fig. 1D) and

motivated downstream assays focused on viral infection efficiency and replication kinetics.

Generation, rescue, and passage stability of s2m-edited PAstV in vitro: Using the PAstV-GX1 RG backbone, s2m edits (Δ25–43, Δ25–33, C12G, C18G) were introduced by splice overlap extension PCR (SOE-PCR). Cloning fidelity was first verified by XhoI/SacII double-digest, which yielded the expected fragment pattern for each construct (Fig. 2A), and then by Sanger reads aligned in SnapGene, confirming the designed edits without unintended changes within the displayed s2m interval (Fig. 2B). Transfection of validated plasmids produced infectious progeny, as evidenced by successful serial passage and maintenance of the engineered signatures: RT-PCR amplicons from P3, P6, and P10 retained the programmed deletions/substitutions with clean base calls at the edited loci and no signal of reversion in the shown region (Fig. 2C). Furthermore, amplification of other genomic regions of the s2m-deficient and mutated strains revealed no mutations in these regions compared to the original strain, suggesting that the genetic changes were confined to the s2m region and did not result in broader genomic alterations.

s2m disruption transiently attenuates PAstV replication: Multi-step growth analyses in PK 15 cells showed that all four s2m mutants (Δ25–43-2, Δ25–33-6, C12G-6, C18G-8) exhibited a reproducible early-phase deficit relative to rPAstV-GX1: infectious titers were significantly lower at 4–12 hpi, but differences diminished from 24 hpi onward and peak yields were comparable through 36–60 hpi (Fig. 3A). ORF2 RT-qPCR corroborated these kinetics, with reduced intracellular viral RNA at 12 hpi and convergence with GX1 by 24 hpi (Fig. 3B). To test generalizability in an intestinal context, we repeated the assay in IPEC-J2 cells under identical conditions (matched virus stocks and MOI). The trajectories closely mirrored those in PK 15: mutants lagged GX1 at 4–12 hpi, whereas by 24 hpi the curves converged and late-phase titers and RNA loads were indistinguishable (Fig. 3C–D). Two-way ANOVA detected a significant effect of genotype during early time points but no genotype×time interaction beyond 24 hpi, indicating that s2m integrity primarily modulates early replication dynamics without measurably altering late-phase output under the conditions tested.

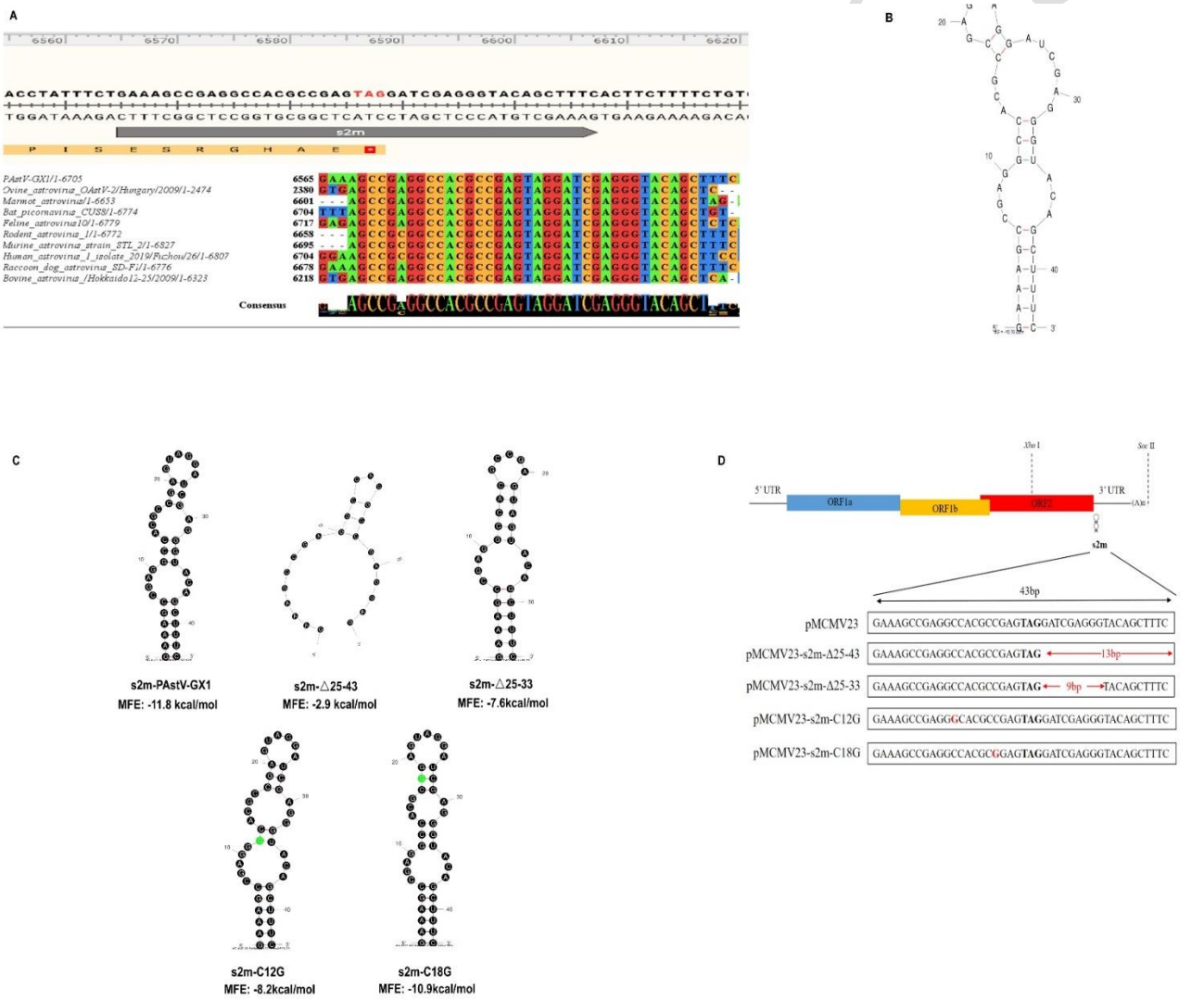

Fig. 1: s2m conservation, structure, and mutagenesis design in PAstV-GX1. (A) Multiple sequence alignment of the s2m element from PAstV-GX1 and representative s2m-containing viruses from other species. (B) Predicted minimum-free-energy secondary structure of the PAstV-GX1 s2m, with stem and loop regions indicated. (C) In silico secondary-structure models for the s2m deletions and point mutations used in this study, highlighting altered pairing relative to wild type. (D) Schematic of the cloning and rescue strategy: location of s2m within the PAstV-GX1 infectious clone, primer design for deletions/mutations, key cloning steps, and recovery of recombinant viruses.

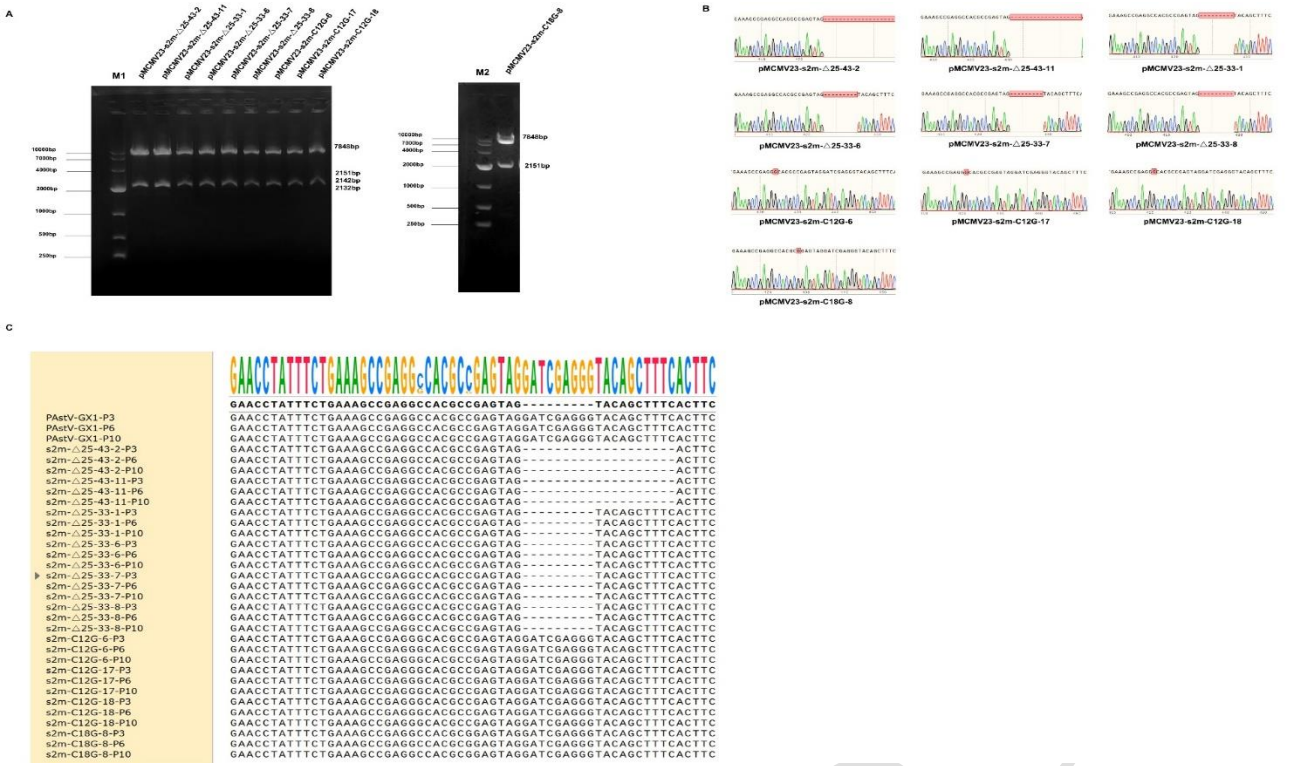

Fig. 2: Construction, verification, and genetic stability of s2m-deletion and point-mutant PAstV-GX1 derivatives. (A) Diagnostic restriction-enzyme digestion of cloned s2m deletion and mutation plasmids; enzyme(s) are indicated above lanes, molecular-weight marker at left, and observed band patterns match the expected fragment sizes for each design. (B) Sanger sequencing of the s2m region in each plasmid confirming the intended deletions/point substitutions and the absence of unintended changes elsewhere in the amplicon (representative alignments shown). (C) Genetic stability of the rescued recombinant viruses after passaging in PK 15 cells: RT-PCR amplification of the s2m-containing 3′UTR followed by sequence alignment illustrates maintenance of engineered edits across passages; the s2m segment is boxed in red).

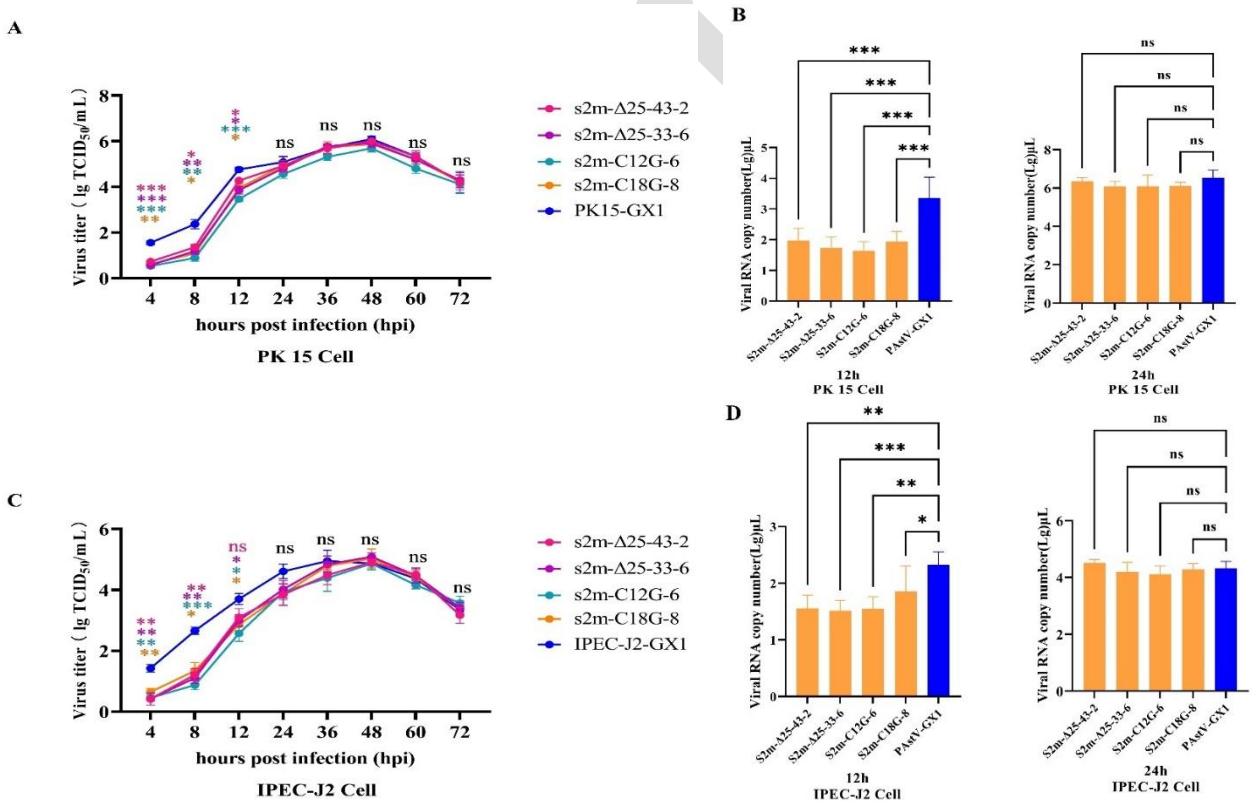

Fig. 3: Multi-step growth kinetics and ORF2 RNA quantification of rPAstV-GX1 and s2m mutant viruses in porcine epithelial cells. (A) PK 15 multi-step growth curves for four s2m mutants (Δ25–43-2, Δ25–33-6, C12G-6, C18G-8) and wild-type rPAstV-GX1 (blue). Cells were infected at MOI 0.01; supernatants were collected at 4, 8, 12, 24, 36, 48, and 60 hpi and titrated as $\log_{10}$ $TCID_{50}$ mL^{-1} by the Reed–Muench method. (B) PK 15 intracellular viral RNA at 12 and 24 hpi measured by RT-qPCR targeting ORF2 and normalized to cell number. (C) IPEC-J2 multi-step growth curves performed under identical conditions to PK 15 (MOI 0.01; time points and titration as in panel A). (D) IPEC-J2 ORF2 RNA at 12 and 24 hpi (as in panel B). Data are means ± s.d. of independent biological replicates (n = 3 per time point). For growth curves, group differences at matched time points were evaluated by two-tailed unpaired Student's t-test; for bar plots, two-tailed unpaired Student's t-test was applied. ns, P>0.05; *P<0.05; **P<0.01; ***P<0.001.

ORF2 Protein Accumulation Dynamics in s2m Mutants: In PK 15 cells infected with WT or s2m variants, FACS demonstrated a uniform early deficit in ORF2 signal across all mutants, with significantly lower ORF2$^+$ frequencies and reduced MFI at 4, 8, and 12 hpi versus WT (Fig. 4A); WB under WT–C18G-8 co-infection corroborated this pattern, showing reduced ORF2 in C18G-8 at 4 and 8 hpi with convergence to WT by 12 hpi (Fig. 4B); concordantly, IFA time courses (4–24 hpi) revealed robust ORF2 in WT by 8 hpi, whereas mutants became clearly positive ≥12 hpi, among which C12G-6 remained the most attenuated (Fig. 4C). These protein-level readouts are consistent with the multi-step growth curves and ORF2 RT-qPCR kinetics indicating s2m-dependent attenuation during the early replication phase and parity with WT at the later sampling point.

Differential Expression of IFN-β in Response to s2m Mutations in PAstV: In PK-15 cells infected with WT or s2m variants, both RT-qPCR and IFN-β promoter dual-luciferase assays showed earlier IFN-β induction in the mutants: differences were evident at 6–10 hpi, peaked at 8 hpi (largest for Δ25–33-6 and C18G-8), and largely converged with WT by 12–24 hpi (Fig. 5A,B). For the VSV-challenge assay, VSV antigen fluorescence was quantified as mean fluorescence intensity (MFI) under matched acquisition settings. Pre-infection with s2m-C18G-8 yielded significantly lower MFI at 8hpi than WT pre-infection, with no difference after 12 hpi (Fig. 5C). Together, these data indicate that s2m mutations enhance early IFN-β responses and coincide with a transient antiviral state, whereas late-phase differences are minimal under the conditions tested.

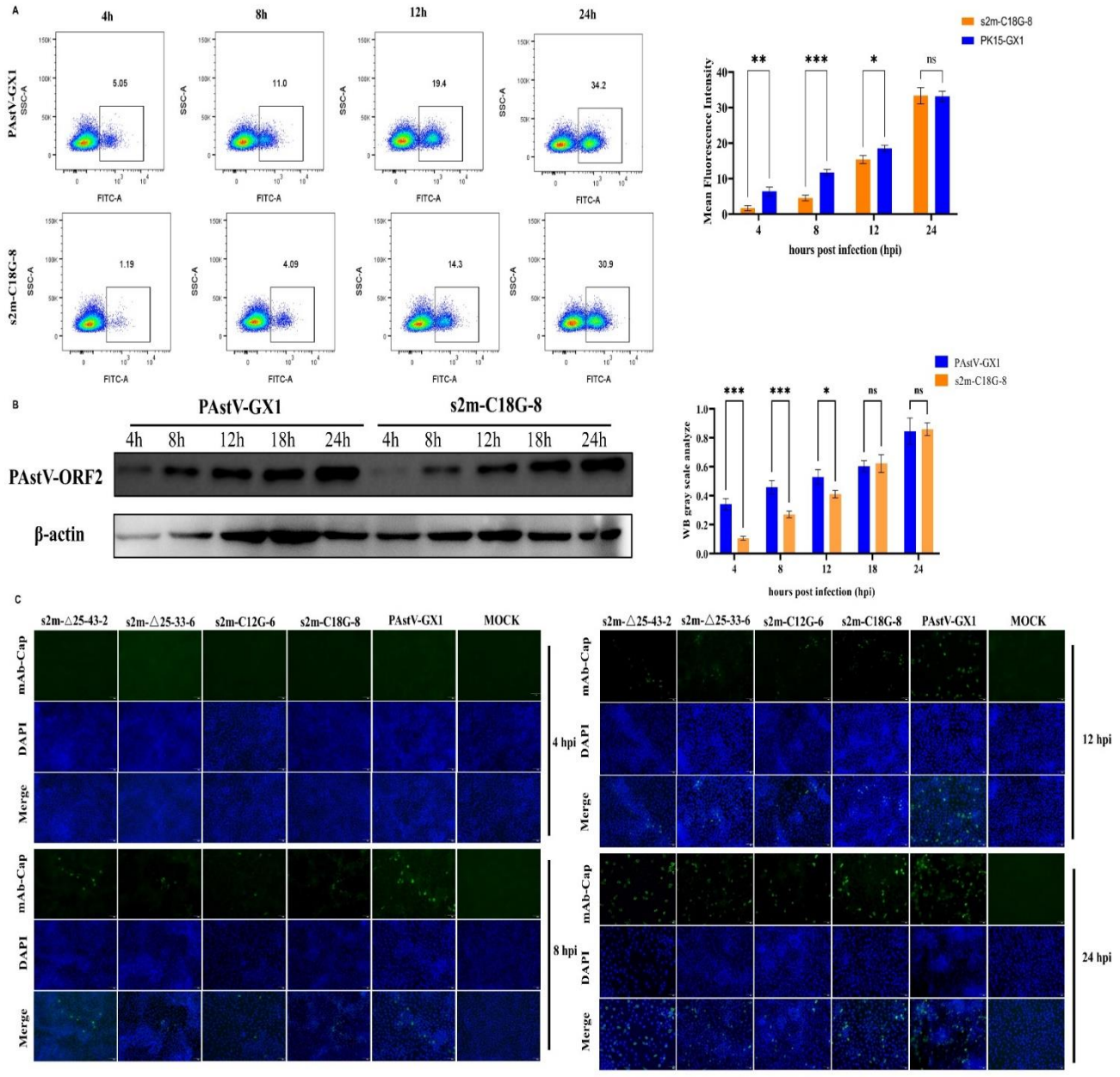

Fig. 4: Temporal profiling of PAstV ORF2 expression in PK 15 cells by flow cytometry, immunoblotting, and immunofluorescence. (A) Flow cytometry of PK 15 cells infected with PAstV-GX1 wild type (WT) or s2m-C18G-8 (MOI = 0.01) and harvested at the indicated hours post-infection (hpi). (B) Western blot analysis of ORF2 in total cell lysates collected at matched time points (loading control: β-actin). (C) Immunofluorescence microscopy of WT and s2m mutant deletion viruses infections at the indicated time points: anti-ORF2 (green) and DAPI (blue). Scale bars, 300μm (10×). Where shown, data represent mean ± s.d. from independent experiments; two-tailed unpaired Student's t-test; ns, P>0.05; *P<0.05; **P<0.01; ***P<0.001.

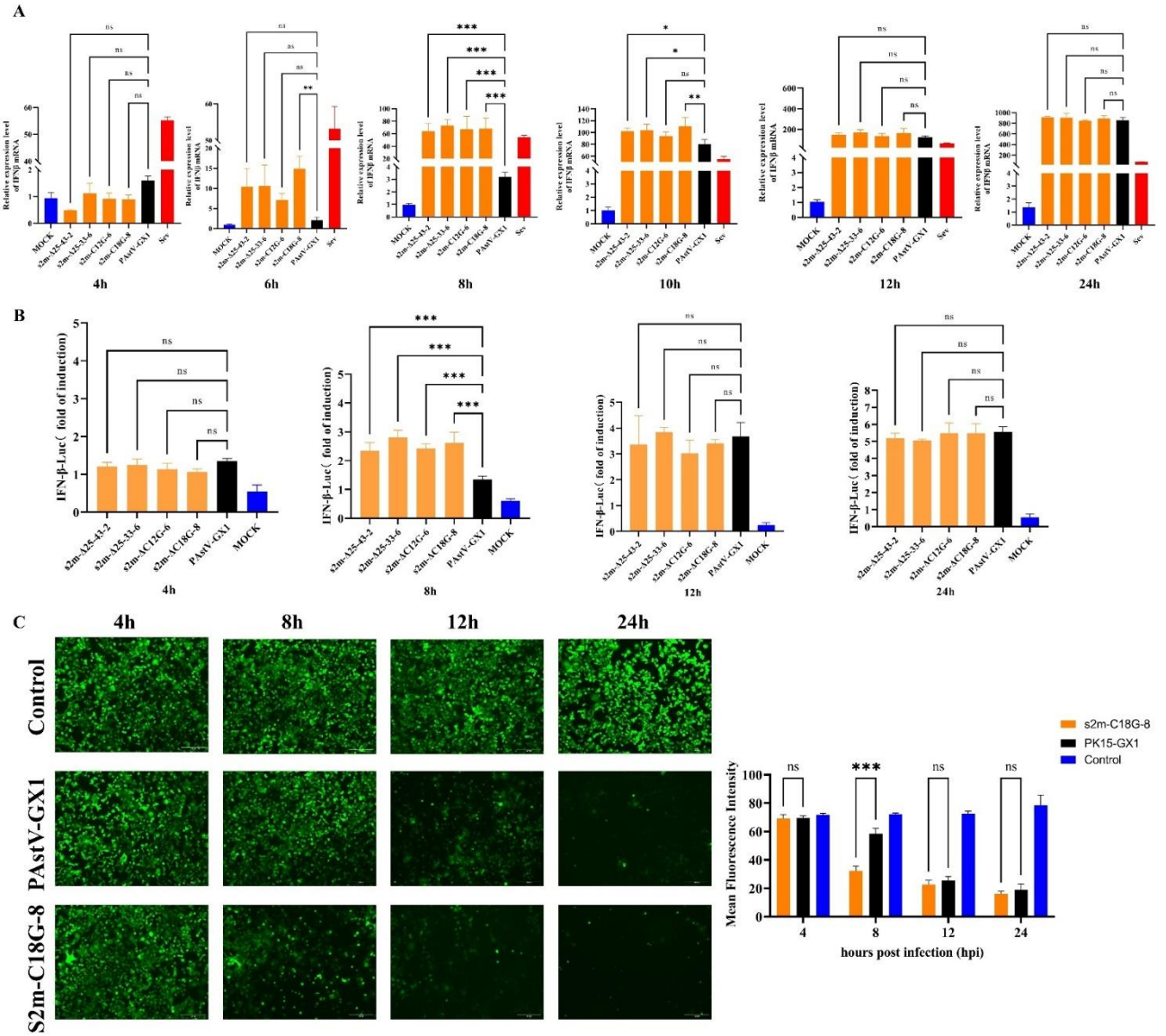

Fig. 5: Time-resolved IFN-β/IFNβ-Luc responses and VSV-GFP challenge in PK-15 cells. (A) RT-qPCR of IFN-β mRNA at 4, 6, 8, 10, 12, and 24 hpi in PK-15 infected with rPAstV-GX1 (WT) or s2m mutants (Δ25–43-2, Δ25–33-6, C12G-6, C18G-8). Values were normalized to GAPDH and plotted as 2^–ΔΔCt relative to time-matched mock. SeV was included as a positive control. (B) IFNβ-Luc assay in PK-15 co-transfected with pIFNβ-Luc (FLuc) and TK-Renilla (RLuc), then infected as in (A). FLuc/RLuc ratios were normalized to time-matched mock. (C) VSV-GFP challenge after PAstV pre-infection (mock, WT, or s2m-C18G-8). Left: GFP fluorescence images at 4, 8, 12, and 24 hpi acquired under identical exposure/gain. Right: quantification as background-subtracted MFI per field. Scale bars, 300 μm (10×). Data are mean ± s.d. from independent experiments (n≥3). Two-tailed unpaired t-test at matched time points; ns, P>0.05; *P<0.05; **P<0.01; ***P<0.001.

DISCUSSION

Our findings underscore the significant role of the Stem-Loop II Motif (s2m) in optimizing viral replication dynamics in PAstV, despite it not being necessary for the virus's lifecycle. Mutants either lacking this structure or with altered s2m demonstrated a notable decrease in replication efficiency, exhibited earlier peak viral titers, and showed reduced overall viral yields in comparison to the parental strain. These observations contrast with research on other RNA viruses, such as SARS-CoV-2, where the s2m motif was identified as non-essential and shown to lack substantial impact on replication kinetics or overall fitness.

An interesting contrast arises when compared to Janowski (Janowski *et al*., 2022), who found that several mutants disrupting s2m in astrovirus VA1 could not be rescued, suggesting a critical requirement for the motif in that virus. In contrast, all PAstV mutants in our study were successfully rescued. We attribute this discrepancy to differences in mutagenesis strategies: while Janowski *et al*. employed more severe deletions that likely disrupted the s2m's secondary structure, our approach retained some structural integrity, allowing for mutant rescue. This suggests that PAstV may tolerate more subtle alterations in the s2m, highlighting its functional flexibility across different viruses.

In our study, the s2m modifications in PAstV were shown to influence replication dynamics and immune response modulation, highlighting the role of the s2m sequence in viral fitness and immune modulation. However, it is important to note that the s2m region is not strictly essential for PAstV replication, as mutations or deletions in this region did not completely abolish viral

replication (Gilbert and Tengs, 2021; Jiang *et al*., 2023). However, our investigation into PAstV reveals that modifications in the s2m motif distinctly influence replication efficiency, viral protein production, and modulation of the immune response. This suggests that s2m functions as a crucial regulatory element, distinctly enhancing viral fitness in a manner specific to the virus (Tengs *et al*., 2013). The influence of s2m on viral growth kinetics and its replication efficiency indicates that this motif plays a considerable role in supporting effective viral replication and maintaining persistence within the host, which extends beyond observations made in related coronaviruses (Gilbert and Tengs, 2021; Imperatore *et al*., 2022; Keep *et al*., 2023; Liu *et al*., 2001). Such insights into the functionality of s2m enrich our understanding of its biological importance in virus-host interactions and viral pathogenesis.

Across PK-15 and IPEC-J2 cells, s2m mutants mainly affected the early phase: differences in IFN-β mRNA levels and IFN-β promoter activity were detectable at 6–10 hpi, peaked around 8 hpi, and narrowed by 12–24 hpi; growth kinetics showed a similar pattern. This timing suggests that s2m chiefly influences the onset of antiviral signaling and early replication rather than late-phase yield. The s2m motif, highly conserved across astroviruses, coronaviruses, and picornaviruses, has been proposed as an antiviral target (Li *et al*., 2008; Manfredonia *et al*., 2020; Tengs and Jonassen, 2016). In PAstV, mutations or deletions within s2m can reduce replication and modulate the host immune response, indicating an important role in viral adaptation and pathogenicity. Notably, Dong *et al*. (2023) reported that PAstV engages the immune sensors RIG-I and MDA5, and the s2m structure may help tune these pathways. Structural changes in s2m may also affect viral RNA stability and translation, with consequences for fitness and transmission. However, our study used only cell lines; without animal data or primary porcine intestinal cells, we can not yet judge effects on gut infection, disease signs, or shedding. In future work, we plan to test s2m mutants in porcine intestinal organoids and in piglets, and to pair these models with focused RIG-I/MDA5 assays to confirm mechanisms and assess the feasibility of s2m-based antivirals.

Advanced techniques such as antisense oligonucleotides or CRISPR-Cas systems offer promising approaches to disrupt s2m functionality (Pickar-Oliver and Gersbach, 2019; Pourshahian, 2021; Ruger *et al*., 2020). Given s2m's role in modulating host immune responses, therapeutically targeting this motif could enhance antiviral defenses and improve the management of viral infections (Cunningham *et al*., 2023b; Lulla *et al*., 2021). Studies on SARS-CoV-2, which demonstrate the dispensability of s2m, support the feasibility of targeting this motif without completely inhibiting viral replication (Jiang *et al*., 2023). This strategy could potentially attenuate viral virulence while enhancing immune recognition, an approach that might be particularly effective in controlling infections by highly pathogenic strains of PAstV and other viruses harboring the s2m motif. Additionally, leveraging these technologies to target s2m could provide novel avenues for the development of antiviral drugs, especially pertinent in the context of global viral spread and pandemics (Graw and Perelson, 2016; Wardeh *et al*., 2024).

Conclusions: Using a reverse-genetics PAstV-GX1 system, we show that the conserved s2m element is dispensable for virus rescue and passage stability but measurably tunes early replication and innate sensing. Deletions and point substitutions within s2m produced viable progeny that replicated more slowly during the first replication cycle and elicited earlier, higher IFN-β transcription and promoter activity, with kinetics converging toward wild type by ~24 h post-infection. Preinfection with an s2m-edited virus transiently restricted a heterologous RNA virus, consistent with an enhanced, short-lived antiviral state. These data support a model in which s2m contributes to the timing and magnitude of PAstV RNA synthesis and/or exposure of pathogen-associated RNA features to RLR pathways, thereby balancing replication efficiency with innate immune evasion. While our conclusions are based on cell-line studies, the combination of genetic viability, phenotypic attenuation early after infection, and immune modulation highlights s2m as a structurally constrained, potentially targetable RNA node.

Funding: This work was supported by the National Natural Science Foundation of China (32260875); Innovation Project of Guangxi Graduate Education (YCBZ2025005); Guangxi Natural Science Foundation (2025GXNSFBA06955).

Acknowledgments: We gratefully acknowledge support from the Guangxi Youth "Shiganjia" Program.

Authors contribution: YL, YL and WH conceived the idea and designed the study. YL and YL were responsible for data curation and methodology development. WZ, YD and SY formal analysis and conducted experimental investigations. QD and WH acquired funding and supervised the project.

REFERENCES

Arias CF, Dubois RM, 2017. The astrovirus capsid: a review. Viruses 9(1):15.

Arruda B, Arruda P, Hensch M, *et al*., 2017. Porcine astrovirus type 3 in central nervous system of swine with polioencephalomyelitis. Emerging Infectious Diseases 23(12): 2097-2100.

Blomstrom AL, Widen F, Hammer AS, *et al*., 2010. Detection of a novel astrovirus in brain tissue of mink suffering from shaking mink syndrome by use of viral metagenomics. Journal of Clinical Microbiology 48(12):4392-4396.

Bonaldo MC, Garratt RC, Caufour PS, *et al*., 2002. Surface expression of an immunodominant malaria protein b cell epitope by yellow fever virus. Journal of Molecular Biology 315(4):873-885.

Cortez V, Margolis E, Schultz-Cherry S, 2019. Astrovirus and the microbiome. Current Opinion in Virology 37:10-15.

Cunningham CL, Frye CJ, Makowski JA, *et al*., 2023a. Effect of the SARS-CoV-2 delta-associated g15u mutation on the s2m element dimerization and its interactions with mir-1307-3p. RNA (New York, N.Y.) 29(11):1754-1771.

Cunningham CL, Frye CJ, Makowski JA, *et al*., 2023b. Effect of the SARS-CoV-2 delta-associated g15u mutation on the s2m element dimerization and its interactions with mir-1307-3p. RNA (New York, N.Y.) 29(11):1754-1771.

De Benedictis P, Schultz-Cherry S, Burnham A, *et al*., 2011. Astrovirus infections in humans and animals - molecular biology, genetic diversity, and interspecies transmissions. Infection, Genetics and Evolution: Journal of Molecular Epidemiology and Evolutionary Genetics in Infectious Diseases 11(7):1529-1544.

Dong Q, Zhu X, Wang L, *et al*., 2023. Replication of porcine astrovirus type 1-infected PK-15 cells in vitro affected by RIG-i and MDA5 signaling pathways. Microbiology Spectrum 11(3): e0070123.

Du Y, Ji C, Liu T, *et al*., 2021a. Identification of a novel protein in porcine astrovirus that is important for virus replication. Veterinary Microbiology 255:108984.

Du Y, Liu T, Qin Y, *et al*., 2021b. Insertion of exogenous genes within the ORF1a coding region of porcine astrovirus. Viruses 13(11):2119.

Fang Q, Wang C, Liu H, *et al*., 2019. Pathogenic characteristics of a porcine astrovirus strain isolated in china. Viruses 11(12):1156.

Gilbert C, Tengs T, 2021. No species-level losses of s2m suggests critical role in replication of SARS-related coronaviruses. Scientific Reports 11(1):16145.

Goebel SJ, Hsue B, Dombrowski TF, *et al*., 2004. Characterization of the RNA components of a putative molecular switch in the 3' untranslated region of the murine coronavirus genome. Journal of Virology 78(2):669-682.

Graw F, Perelson AS, 2016. Modeling viral spread. Annual Review of Virology 3(1):555-572.

Huston NC, Wan H, Strine MS, *et al*., 2021. Comprehensive in vivo secondary structure of the SARS-CoV-2 genome reveals novel regulatory motifs and mechanisms. Molecular Cell 81(3):584-598.

Imperatore JA, Cunningham CL, Pellegrene KA, *et al*., 2022. Highly conserved s2m element of SARS-CoV-2 dimerizes via a kissing complex and interacts with host miRNA-1307-3p. Nucleic Acids Research 50(2):1017-1032.

Janowski AB, Jiang H, Fujii C, *et al*., 2022. The highly conserved stem-loop II motif is important for the lifecycle of astroviruses but dispensable for SARS-CoV-2. BioRxiv: the preprint server for biology.

Jiang H, Joshi A, Gan T, *et al*., 2023. The highly conserved stem-loop II motif is dispensable for SARS-CoV-2. Journal of Virology 97(6):e0063523.

Keep S, Dowgier G, Lulla V, *et al*., 2023. Deletion of the s2m RNA structure in the avian coronavirus infectious bronchitis virus and human astrovirus results in sequence insertions. Journal of Virology 97(3):e0003823.

Kofstad T, Jonassen CM, 2011. Screening of feral and wood pigeons for viruses harbouring a conserved mobile viral element: characterization of novel astroviruses and picornaviruses. PloS One 6(10):e25964.

Li L, Kang H, Liu P, *et al*., 2008. Structural lability in stem-loop 1 drives a 5' UTR-3' UTR interaction in coronavirus replication. Journal of Molecular Biology 377(3):790-803.

Liu H, Hu D, Zhu Y, *et al*., 2020. Coinfection of parvovirus and astrovirus in gout-affected goslings. Transboundary and Emerging Diseases 67(6):2830-2838.

Liu Q, Johnson RF, Leibowitz JL, 2001. Secondary structural elements within the 3' untranslated region of mouse hepatitis virus strain JHM genomic RNA. Journal of Virology 75(24):12105-12113.

Liu T, Liao Y, Du Y, *et al*., 2023. Insertion of exogenous genes within the ORF1b coding region of porcine astrovirus. Veterinary Microbiology 280:109675.

Lulla V, Wandel MP, Bandyra KJ, *et al*., 2021. Targeting the conserved stem loop 2 motif in the SARS-CoV-2 genome. Journal of Virology 95(14):e0066321.

Manfredonia I, Nithin C, Ponce-Salvatierra A, *et al*., 2020. Genome-wide mapping of SARS-CoV-2 RNA structures identifies therapeutically-relevant elements. Nucleic Acids Research 48(22):12436-12452.

Mendenhall IH, Smith GJ, Vijaykrishna D, 2015. Ecological drivers of virus evolution: astrovirus as a case study. Journal of Virology 89(14):6978-6981.

Pfaff F, Schlottau K, Scholes S, *et al*., 2017. A novel astrovirus associated with encephalitis and ganglionitis in domestic sheep. Transboundary and Emerging Diseases 64(3):677-682.

Pickar-Oliver A, Gersbach CA, 2019. The next generation of CRISPR-cas technologies and applications. Nature reviews. Molecular Cell Biology 20(8):490-507.

Porto PS, Rivera A, Moonrinta R, *et al*., 2023. Entry and egress of human astroviruses. Advances in Virus Research 117:81-119.

Pourshahian S, 2021. Therapeutic oligonucleotides, impurities, degradants, and their characterization by mass spectrometry. Mass Spectrometry Reviews 40(2):75-109.

Qin Y, Fang Q, Liu H, *et al*., 2018. Construction of a reverse genetic system for porcine astrovirus. Archives of Virology 163(6):1511-1518.

Reuter G, Pankovics P, Boros A, 2018. Nonsuppurative (aseptic) meningoencephalomyelitis associated with neurovirulent astrovirus infections in humans and animals. Clinical Microbiology Reviews 31(4):e00040-18.

Rivera R, Nollens HH, Venn-Watson S, *et al*., 2010. Characterization of phylogenetically diverse astroviruses of marine mammals. The Journal of General Virology 91(Pt 1):166-173.

Robertson MP, Igel H, Baertsch R, *et al*., 2005. The structure of a rigorously conserved RNA element within the SARS virus genome. PLoS Biology 3(1):e5.

Ruger J, Ioannou S, Castanotto D, *et al*., 2020. Oligonucleotides to the (gene) rescue: FDA approvals 2017-2019. Trends in Pharmacological Sciences 41(1):27-41.

Stanic M, 1963. A simplification of the estimation of the 50 percent endpoints according to the Reed and Muench method. Pathologia Et Microbiologia 26:298-302.

Tengs T, Jonassen CM, 2016. Distribution and evolutionary history of the mobile genetic element s2m in coronaviruses. Diseases (Basel, Switzerland) 4(3):27.

Tengs T, Kristoffersen AB, Bachvaroff TR, *et al*., 2013. A mobile genetic element with unknown function found in distantly related viruses. Virology Journal 10:132.

Ulloa JC, Gutierrez MF, 2010. Genomic analysis of two ORF2 segments of new porcine astrovirus isolates and their close relationship with human astroviruses. Canadian Journal of Microbiology 56(7):569-577.

Wardeh M, Pilgrim J, Hui M, *et al*., 2024. Features that matter: evolutionary signatures can predict viral transmission routes. PLoS Pathogens 20(10):e1012629.

Zhang W, Wang W, Liu X, *et al*., 2021. Identification of novel b-cell epitopes on the capsid protein of type 1 porcine astrovirus, using monoclonal antibodies. International Journal of Biological Macromolecules 189:939-947.